Environmental Science & Technology

Article

pubs.acs.org/est

Coastal Acidification Induced by Tidal-Driven Submarine Groundwater Discharge in a Coastal Coral Reef System

Guizhi Wang, Wenping Jing, Shuling Wang, Yi Xu, Zhangyong Wang, Zhouling Zhang, Quanlong Li, and Minhan Dai*

State Key Laboratory of Marine Environmental Science, Xiamen University, Xiamen 361005, China

Supporting Information

ABSTRACT: We identified a barely noticed contributor, submarine groundwater discharge (SGD), to acidification of a coastal fringing reef system in Sanya Bay in the South China Sea based on time-series observations of Ra isotopes and carbonate system parameters. This coastal system was characterized by strong diel changes throughout the spring to neap tidal cycle of dissolved inorganic carbon (DIC), total alkalinity, partial pressure of CO_2 (pCO_2) and pH, in the ranges of 1851−2131 μmol kg^{-1}, 2182−2271 μmol kg^{-1}, 290−888 μatm and 7.72−8.15, respectively. Interestingly, the diurnal amplitudes of these parameters decreased from spring to neap tides, governed by both tidal pumping and biological activities. In ebb stages during the spring tide, we observed the lowest salinities along with the highest DIC, pCO_2 and Ra isotopes, and the lowest pH and aragonite saturation state. These observations were consistent with a concurrent SGD rate up to 25 and 44 cm d^{-1}, quantified using Darcy's law and ^{226}Ra, during the spring tide ebb, but negligible at flood tides. Such tidal-driven SGD of low pH waters is another significant contributor to coastal acidification, posing additional stress on coastal coral systems, which would be even more susceptible in future scenarios under higher atmospheric CO_2.

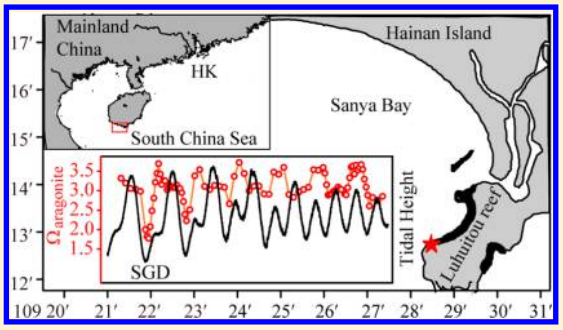

1. INTRODUCTION

The atmospheric carbon dioxide (CO_2) concentration has been increasing over the past 260 years from approximately 280 ppm in the preindustrial time to nearly 400 ppm at present.[1] Due to the rapid air-sea exchange of CO_2, the concentration of CO_2 in the surface ocean has also risen, resulting in a shift in its chemical equilibrium[2] and an unprecedented rapid decline in surface seawater pH, referred to as ocean acidification.[3] Marine calcifying organisms can be adversely impacted by the decrease in seawater pH along with decreases in carbonate ion concentration and production of calcium carbonate ($CaCO_3$).[3] Corals, which form reefs from aragonite, are well recognized to be threatened by ocean acidification due to decreased skeletal formation in reef-building corals under lower pH conditions.[3] On average, a doubling of preindustrial atmospheric CO_2 concentration is expected to result in about a 10−50% decrease in the calcification rate of reef-building corals.[4]

Coastal coral systems may also be affected by acidification due to seasonal upwelling of undersaturated waters onto continental shelves[5] and release of CO_2 from volcanic vents under the sea.[6] Moreover, local land-based forcing may affect coastal coral systems through nutrient loading from watershed fertilization and sewage discharge.[7] One pathway of these inputs is via submarine groundwater discharge (SGD).[8]

Owing to microbial respiration in coastal aquifers where meteoric groundwater and seawater that has infiltrated the aquifer mix, SGD is commonly characterized by high concentrations of dissolved inorganic carbon (DIC), high partial pressure of CO_2 (pCO_2), and low pH compared with the receiving coastal water bodies.[9−12] SGD has also been shown to be a major source of alkalinity to a fringing coral reef lagoon, which may potentially buffer against ocean acidification.[13] However, tidally driven seawater recirculation (a type of SGD[10]) in carbonate sands[14] is demonstrated to drive down the pH in coral reefs.[9] Significant correlations between SGD signals and pH values have been demonstrated, with the contribution of SGD to a coral reef system estimated based on SGD end-member values.[9,15] Due to the complexity of pH changes in coastal reef systems, which are affected by multiple drivers, our mechanistic understanding remains limited with only a few studies conducted in a limited number of reef types.[9,14,15] Moreover, quantitative studies have been particularly lacking.

Through time-series observations of carbonate system parameters, this study sought to examine if SGD contributes to acidification of a coastal fringing reef setting characterized by insignificant river runoff during a dry season. Naturally occurring radium isotopes were applied as SGD tracers to quantify the SGD rates. We showed that tidal-driven SGD was the main driver of coastal acidification in the fringing reef

Received: June 27, 2014
Revised: October 13, 2014
Accepted: October 22, 2014
Published: October 22, 2014

   dx.doi.org/10.1021/es5026867 | Environ. Sci. Technol. 2014, 48, 13069−13075

system, which could make the reef system more susceptible to increasing atmospheric CO_2.

2. MATERIALS AND METHODS

2.1. Study Area. Our coastal time-series station CT is located at the Luhuitou fringing reef, situated along the west coast of the Luhuitou Peninsula in southeast Sanya Bay of Hainan Island in the northern South China Sea (Figure 1). It is

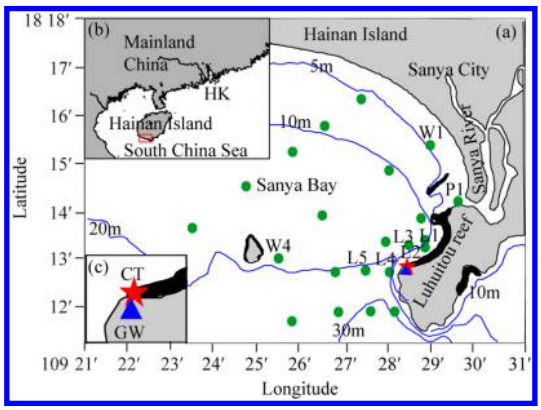

Figure 1. Study area. (a) Map of Sanya Bay showing the sampling stations. Inserted are (b) the map of the northern South China Sea, showing the location of Sanya Bay at the southern tip of Hainan Island, and (c) Stations CT and GW. The green dots are mapping stations in Sanya Bay, the red star represents the coastal time-series station CT, and the blue triangle is the groundwater station GW. The blue lines are the isobaths, and the black areas are the fringing coral reefs.

about 60 m away from the onshore sampling platform with an average water depth of 1.80 m. The groundwater monitoring station GW, a domestic well 2.05 m deep with a 1 m radius, is ~100 m away from Station CT. The Luhuitou fringing reef is a leeward coast with low wave energy. It is ~3 km long and 250–500 m wide.[16] This coral system is economically important to the region, but has been experiencing rapid degradation since the 1960s. In 2009, the mean coral cover was 12% as compared to 90% in the 1960s.[17] The reason for such a dramatic decline in corals is unclear, but likely due to both anthropogenic activities in the region and climate change.[18] The ecosystem is dominated by coralline algae with lower diurnal ranges in pCO_2, pH and DO in winter than in the other seasons.[19]

The annual mean sea surface temperature (SST) in Sanya Bay is 26.8 °C, and the annual precipitation is around 1600–1800 mm.[16] Irregular diurnal tides dominate, with a mean tidal range of 0.90 m and the largest of 2.14 m.[16] To the north of the Luhuitou fringing reef, the Sanya River discharges into Sanya Bay with an annual average discharge of 5.86 $m^3\ s^{-1}$.[20] 95% of the rainfall occurs in May to October.[21] The Bay is oligotrophic because of the influence of the northern South China Sea, which is known for oligotrophy.[22] The Sanya River is the main nutrient source for the Bay, leading to the highest phytoplankton and bacterioplankton biomass near the estuary and decreasing seaward.[23] Multiple habitats (coral reefs, mangroves, mudflats, rocky and sandy beaches) occur in the Bay, with coral reefs accounting for 30% of the coastline.[24] Holocene deposits of coral debris, sand and silt surround the coast,[25] forming the surficial unconfined aquifer.[26]

2.2. Sampling and Measurements. Time series observations of temperature, salinity, water depth, DIC, total alkalinity (TA), pH (in total scale), dissolved oxygen (DO) and dissolved radium were carried out during February 6–13, 2012 at Stations CT and GW. Well water was pumped at the fastest rate possible at Station GW to estimate hydraulic parameters from the recovery of water in the well. A mapping cruise in Sanya Bay (Figure 1) was carried out during February 2–3, 2012 to evaluate the influence of the Sanya River and to constrain the end-member of the offshore water. Details of the deployments of sampling, analytical methods and carbonate chemistry calculations are provided in the Supporting Information (SI).

2.3. SGD Rate Estimation Using ^{226}Ra Time-Series Observations. The discharge rate from the coastal aquifer was estimated using a nonsteady state procedure with ^{226}Ra time-series data. Briefly, changes in the ^{226}Ra inventories with time were converted to fluxes after taking account of tidal effects and mixing with offshore waters, which were then divided by the concentration of ^{226}Ra in the groundwater to obtain a discharge rate (See SI).

3. RESULTS

3.1. Environmental Parameters in Sanya Bay. Surface seawater salinity varied within a small range, 33.60–33.89, slightly lower in the north and northeast off the Sanya River mouth than in southern Sanya Bay (Figure S1a, SI). Such differences in salinity were also observed from the vertical profiles measured at Stations P1, L1, L2, L3, W1, and W4, which demonstrated again slightly lower salinity at Stations P1 and W1 (Figure S1c, SI), indicating weak influence of the Sanya River plume. The salinity at river-influenced stations, P1 and W1, seemed to be separated from that around Station CT (i.e., Stations L1–3) by the offshore salinity at W4. Note that all of the vertical profiles shown in Figures S1b-c (SI) suggested that water in Sanya Bay near Luhuitou fringing reef, especially around Station CT, was relatively homogeneous in February with the vertical differences in temperature less than 0.10 °C and in salinity less than 0.10 except at Station L1, where a 0.20 °C lower temperature and 0.20 greater salinity were found at the surface than at the bottom. Note also that the north of the Bay was investigated on February 2 and the south of the Bay on February 3, both of which covered an ebb-flood tidal cycle with the maximum salinity on both days coincident with the lowest tides. This indicated that the salinity variation was not caused by tides, and the Sanya River plume was confined in the northern part of the Bay.

At offshore stations around CT (i.e., Stations L1–5), the pH and concentrations of DIC and TA were nearly constant at 8.07 ± 0.00, 1942 ± 1 μmol kg^{-1} and 2219 ± 2 μmol kg^{-1} (n=10) during our sampling period, respectively (Table S1, SI). Station CT seemed to be unaffected by the river plume water that was slightly higher in DIC and lower in TA and pH (Figure S2, Table S1, SI). There was no difference in these parameters between sites north (Stations L1–3) and south (Stations L4–5) of Station CT.

3.2. Time-Series Observations at the Coral Reef Station CT. During the week-long observations, Station CT had an irregular diurnal tide, with a daily tidal range decreasing from 1.40 m during the spring tide to 0.65 m during the neap tide (Figure 2a). Temperature varied with a solar radiation-dominated diurnal trend, with peak temperatures appearing in the middle of the day. The average temperature was 23.00 °C and a maximum diel variation of 1.55 °C was observed during the spring tide. The salinity dropped sharply during the ebb

dx.doi.org/10.1021/es5026867 | Environ. Sci. Technol. 2014, 48, 13069–13075

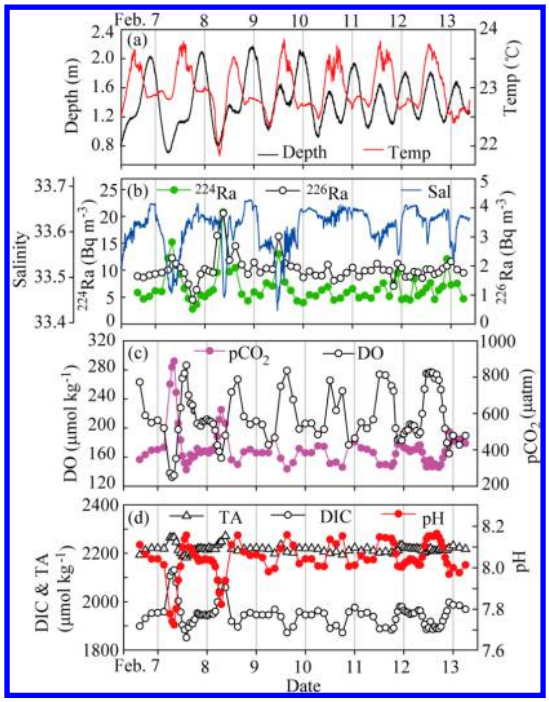

Figure 2. Time series observations at Station CT in the Luhuitou fringing reef of Sanya Bay, China during February 6–13, 2012. (a) Water depth and temperature (Temp), (b) salinity (Sal), ^{224}Ra and ^{226}Ra, (c) DO and pCO_2, (d) pH, DIC and TA. Lines connecting the symbols are to show trends.

flow of the spring tide, from 33.67 to 33.43, whereas during the neap tide the diurnal variation was from 33.65 to 33.54 (Figure 2b). pH and DO showed similar trends to salinity during the spring tide, with pH dropping from 8.15 during the flood tide to a minimum of 7.72 during the ebb flow and DO concentration decreasing from the maximum of 286 μmol kg^{-1} during the flood tide to the lowest of 135 μmol kg^{-1} during the ebb flow (Figures 2c-d). During the neap tide, pH and DO followed more of a diel pattern, with much less diurnal variations (from 0.17 to 0.20 for pH and from 89 to 112 μmol kg^{-1} for DO). Meanwhile, during the spring tide pCO_2, DIC and TA reached their peak values of 888 μatm, 2131 μmol kg^{-1} and 2271 μmol kg^{-1}, respectively during the ebb flow and their minima, 290 μatm, 1851 μmol kg^{-1} and 2182 μmol kg^{-1} during the flood tide. During the neap tide their diurnal variations were relatively small, 100 μatm for pCO_2, 104 μmol kg^{-1} for DIC, and 32 μmol kg^{-1} for TA. DIC varied more with tides than TA (Figure 2d). The activities of ^{224}Ra and ^{226}Ra were higher during ebb flows than during flood tides with the maxima, 20.8 Bq m^{-3} and 3.8 Bq m^{-3}, appearing during the spring tide. The diurnal variations were 16.5 Bq m^{-3} for ^{224}Ra and 2.1 Bq m^{-3} for ^{226}Ra during the spring tide and were about half as much during the neap tide (Figure 2b). Using the maximum ^{226}Ra activity in the well of 61 Bq m^{-3} (Table S2, SI), SGD into Station CT was calculated to vary in the range of 0–44 cm d^{-1} (0–5.1 × 10^{-6} m s^{-1}) with an average of 15 ± 10 cm d^{-1} (Figure S3, SI), comparable to discharge rates in other coral reef systems.[14,15] The highest SGD rate appeared during the spring tide. The rates correlated with salinity and tidal height: lower salinity and tidal height coincided with greater groundwater seepage rate.

3.3. Observations at the Groundwater Station. From the spring to neap tide, diurnal variations in the water level and temperature were relatively small, at most 0.60 m for water level and 0.20 °C for temperature, and had no obvious trends when the recovery periods were not considered (Figure S4, Table S3, SI). Salinity had no apparent trend in its diurnal variation during the spring tide (Table S2, SI) with an average of 19.95 ± 0.25. The average temperature in the well was 26.80 ± 0.06 °C (the uncertainty represents one standard deviation), with the recovery periods included. These results indicated that groundwater properties were relatively constant with time, without apparent tidal resonances. Diel variations of DIC and TA in the well during the spring tide were 229 μmol kg^{-1} and 114 μmol kg^{-1} (Figure S5a, SI), smaller than their variations measured at Site CT. The average DIC and TA values of the groundwater during the spring tide were 5764 ± 98 μmol kg^{-1} (n = 12) and 5589 ± 39 μmol kg^{-1} (n = 13). The pH ranged from 7.13 to 7.16 with an average of 7.14 ± 0.01 (n = 13). DO varied from 78 to 111 μmol kg^{-1} with an average of 104 ± 9 μmol kg^{-1} (n = 12) (Figure S5b, SI), about half of the DO concentration at Site CT. Activities of Ra were relatively constant except for the sample GW1, 104 ± 4 Bq m^{-3} for ^{224}Ra and 41 ± 2 Bq m^{-3} for ^{226}Ra with GW1 excluded.

4. DISCUSSION

4.1. What Affects Diurnal and Tidal Variations in the Parameters at the Coastal Reef Site? The daily minimum salinity at Station CT appeared during the ebb flow, as low as 33.43 during the spring tide and 33.54 during the neap tide. This suggests that more freshwater input into the fringing reef environment occurs during the ebb flow of the spring tide than during that of the neap tide. The Sanya River plume affected the northeast of the Bay with little impact on Station CT. Precipitation would unlikely cause spring-neap changes in salinity. The only other source of fresh water at this site would be groundwater discharge. The coincidence of the peaks of DIC and TA with the daily minima in salinity, DO and pH indicate that the freshwater end-member was of low salinity, pH and DO, and of high DIC and TA, which were characteristics of the nearby groundwater. In addition, the daily minimum salinity and maximum activities of ^{224}Ra and ^{226}Ra co-occurred during the spring tide. This suggests that the highest SGD occurred during the ebb flow of the spring tide, bringing more groundwater into the coastal fringing reef system.

Under the influence of tidal-driven SGD, variations in pH, DO, pCO_2, DIC and TA during the spring tide could be as large as 0.43 pH units, 154 μmol kg^{-1}, 598 μatm, 179 μmol kg^{-1} and 82 μmol kg^{-1}, respectively and followed a tidal pattern. However, around the neap tide, when salinity stayed almost constant, pH, DO, pCO_2, DIC and TA showed less, but distinct, diurnal variability over a day-night cycle. The pH varied from 7.97 to 8.16, and DO from 183 μmol kg^{-1} to 275 μmol kg^{-1}. Both pH and DO increased during the daytime with the maximum occurring around 18:00, and decreased at night to a minimum at 08:00. The pCO_2, DIC and TA varied inversely with pH and DO in range of 280–420 μatm, 1882–1979 μmol kg^{-1} and 2198–2220 μmol kg^{-1}, respectively. This diel cycle reflected biological dominance on DO and the carbonate system during the neap tide. Such great diel changes are commonly observed in other coral reef systems. For example, in the coral reef system at Xishan Island in the South China Sea, the diurnal variation in pCO_2 is as high as 608 μatm, which is dominated by biological metabolism.[27] In Nanwan Bay, a fringing reef system in Taiwan, diurnal variations are 96–234 μmol kg^{-1} for DIC, 89–422 μatm for pCO_2, and 37–239

dx.doi.org/10.1021/es5026867 | Environ. Sci. Technol. 2014, 48, 13069–13075

μmol kg^{-1} for DO, which are driven mainly by the net ecosystem production.[28] The broadest diel ranges, DO: 28−463 and pH: 7.69−8.44, are found in a reef lagoon in the Great Barrier Reef, which are driven by SGD and biological metabolism.[9]

Biological controls on the carbonate system and oxygen in coral reef systems include organic and inorganic carbon metabolism.[28] During organic carbon metabolism, photosynthesis consumes DIC and releases oxygen at a Redfield ratio of 106:138, with TA decreasing by a ratio to DIC of 17:106, so that DO increases in the surrounding water, while respiration causes DO to decrease and DIC and TA to increase proportionally. During inorganic carbon metabolism, calcification by corals decreases DIC and TA at a ratio of 1:2 and increases pCO_2 in the surrounding water, but it has no effect on DO. Therefore, in the daytime, photosynthesis caused the maximum DO and a lower DIC, and respiration at night resulted in the minimum DO and a higher DIC. The slope of linear regression between DO and DIC during the neap tide was −0.98 with r^2 of 0.91 (Figure S6, SI), indicating that DO and DIC changed by a ratio lower than the Redfield ratio of 138:106. This implied that, besides organic carbon metabolism, calcification might also be involved in regulating the carbonate system.

Overall, the carbonate system parameters in this coastal coral reef system showed distinct diurnal variations from spring to neap tide, with more pronounced diurnal variations during the spring tide. In contrast, diurnal variability in the reef system in Nanwan Bay, Taiwan is predominantly controlled by the net ecosystem production of the benthic-dominated nearshore ecosystem, and diminishes toward the spring tide owing to intensified dispersion from tidal advection.[28] The greater diurnal variations in our study, however, were associated with more groundwater inputs into the coastal coral reef system during the ebb flows of the spring tide. Diurnal variability observed in two coral reef lagoons at Rarotonga, Cook Islands and Heron Island, Great Barrier Reef was explained similarly by both biological and SGD drivers, but at Rarotonga SGD with high concentrations of carbonate species was the dominant driver and at Heron Island biological activities stimulated by high nutrient and organic loads from SGD played the predominant role.[15]

4.2. Quantify Different Contributors to the Variations in the Carbonate System. To differentiate contributions of SGD and biological activities to the carbonate system, a closer look was taken at the DIC, TA and salinity during the falling and rising phases of the spring tide. The DIC and TA showed different behavior during these two phases. During the ebb flow, with a faster falling speed characterized by a shorter ebb time, both DIC and TA behaved conservatively (Figure 3), showing mixing between the offshore water with a salinity of 33.67 and SGD with a salinity of ∼19.95. The offshore water end-member had DIC and TA values of ∼1942 μmol kg^{-1} and 2219 μmol kg^{-1}, which were designated as DIC_O and TA_O. During the spring tide, DIC and TA of the groundwater almost linearly varied with salinity in the range 5594−5905 μmol kg^{-1} and 5531−5636 μmol kg^{-1}, respectively (Figure S7a, SI). At flood tide in the daytime during the spring tide, however, both DIC and TA showed a strong removal signal (Figure 3), and the offsets of DIC and TA between conservative mixing lines and observations were as large as 172 μmol kg^{-1} and 50 μmol kg^{-1}, respectively. This consumption of DIC and TA was most likely caused by strong photosynthesis and calcification in the daytime. Consequently, contributions of SGD and biological activities and of inorganic and organic carbon metabolisms to the carbon system parameters were quantitatively differentiated using a mixing model (see SI).

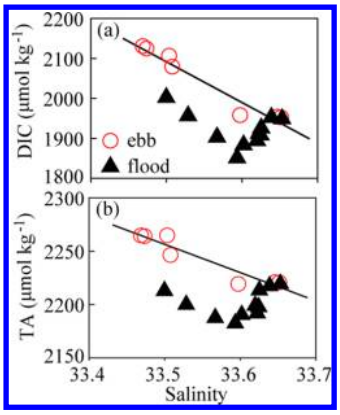

Figure 3. Behaviors of DIC and TA with salinity during the ebb flow and flood tide of the spring tide at Station CT. (a) DIC, the linear regression between DIC and salinity was $y = -1047.39\,x + 37184$ with r^2 of 0.96, (b) TA, the linear regression equation was $y = -273.16\,x + 11408$ with r^2 of 0.92.

Biological activities and SGD regulated the carbonate system differently in the coral reef system. TA and DIC contributed by SGD, ΔTA_{SGD} and ΔDIC_{SGD}, showed significant tidal variations, greater during the spring tide than during the neap tide, ranging from −7 to 88 μmol kg^{-1} and from −24 to 237 μmol kg^{-1}, respectively (Figure 4a). The ratio of change, that is, the regression slope, between TA and DIC due to SGD inputs was 0.37 with r^2 of 1.00 (Figure S8, SI). This ratio was very close to the slope of linear regression between TA vs DIC in the groundwater, 0.35 (Figure S7b, SI), and confirmed the validity of the mixing calculations. Most ΔDIC_{SGD} and ΔTA_{SGD} were positive with spring-neap and ebb-flood tidal signals, indicating net inputs of DIC and TA via SGD induced by tidal pumping. The few negative values, which occurred during flood tides, indicated seawater intrusion into the coastal aquifer, that is, negative SGD rates. The TA and DIC impacted by biological activities, TA_{bio} and DIC_{bio}, were linearly correlated with a slope of 0.25 and r^2 of 0.74 (Figure S9, SI), indicating that organic metabolism, or photosynthesis/respiration, but not inorganic metabolism, or calcification/dissolution, was the major biological activity affecting the carbonate system with calcification accounting for about 12.5% of biologically impacted DIC. TA and DIC contributed by biological activities, ΔDIC_{bio} and ΔTA_{bio}, ranged from −210 to 101 μmol kg^{-1} and from −52 to 25 μmol kg^{-1}, respectively, mostly negative in the daytime and positive at night with smaller magnitudes (Figure 4a), reflecting strong photosynthesis and calcification in the daytime. Besides the day-night cycle, daily minima of ΔDIC_{bio} and ΔTA_{bio} were a little lower around the spring tide than around the neap tide, demonstrating tidal effects most likely associated with SGD inputs. The highest consumption of DIC by biological activities coincided with the greatest amount of DIC input by SGD on February 9. This enhanced production was likely induced by higher nutrient inputs via SGD. Under the highest consumption, even assuming that all DIC consumed was from SGD, there would still be excess DIC of 26 μmol kg^{-1} in the system due to SGD. Therefore, during the spring tide, SGD mainly induced by tidal pumping played a predominant role in regulating variations of carbonate parameters in this coastal

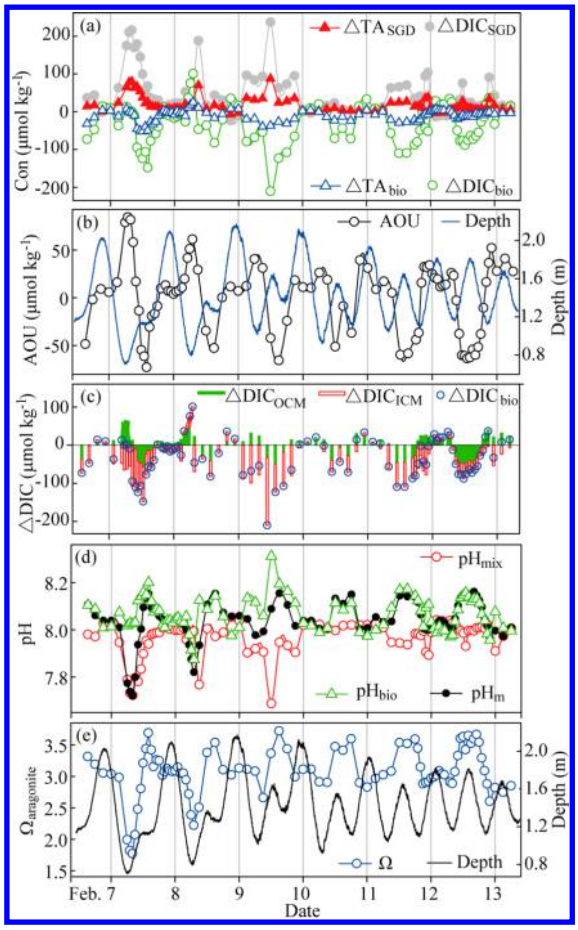

Figure 4. Diurnal variations of calculated DIC, TA, AOU, pH, and aragonite saturation state (Ω) in a spring-neap tidal cycle during February 6–13, 2012 at Station CT in the Luhuitou fringing reef. (a) DIC and TA contributed by groundwater discharge (SGD) and biological activities (bio), (b) AOU and water depth, (c) biologically contributed DIC (ΔDIC_{bio}), which is the sum of that contributed by organic metabolism (ΔDIC_{OCM}) and that by inorganic metabolism (ΔDIC_{ICM}), (d) pH measured (pH_m), pH calculated from DIC_{bio} and TA_{bio} (pH_{bio}), and pH calculated from DIC_{mix} and TA_{mix} (pH_{mix}), (e) Ω and water depth. Lines connecting the symbols are to show trends.

coral reef system. During the neap tide, biological activities were the major drivers controlling the carbonate parameters.

Changes in DIC due to photosynthesis/respiration could be estimated using the apparent oxygen utilization (AOU). The AOU showed a day-night cycle with bigger diel variations during the spring tide, from −72 to −84 μmol kg^{-1}, than during the neap tide, from −64 to −52 μmol kg^{-1} (Figure 4b). AOU was positive at night, indicating oxygen consumption by respiration, while in the daytime AOU was negative, implying much greater photosynthetic rates than respiration rates. Accordingly, the DIC produced by organic carbon metabolism, ΔDIC_{OCM}, showed similar diurnal and tidal patterns (Figure 4c), varying from −56 to 65 μmol kg^{-1} during the spring tide and from −49 to 40 μmol kg^{-1} during the neap tide. The DIC produced by inorganic carbon metabolism, ΔDIC_{ICM}, however, was mostly negative, with a minimum of −178 μmol kg^{-1}, indicating uptake of DIC by calcification in the system. During the spring tide there seemed to be more calcification going on with more negative ΔDIC_{ICM} than during the neap tide. The highest DIC consumption on February 9 was due to the greatest calcification, since ΔDIC_{OCM} was almost the same as that at the same time on the other days. A few positive ΔDIC_{ICM} values appeared at night or in early mornings, representing dissolution of $CaCO_3$ at these times.

4.3. SGD Rates at Station CT Estimated Using Darcy's Law. The estimated SGD rates using ^{226}Ra and the nonsteady state technique were always 0 or positive because of the assumption of the most negative flux as the mixing flux. At Station CT, however, negative ΔDIC_{SGD} during high tides implied negative SGD rates. An attempt was made using Darcy's law to capture these negative SGD (see SI). The estimated seepage rate at Station CT was 11 ± 6 cm d^{-1}, on average, almost the same as the average rate estimated using ^{226}Ra, 15 ± 10 cm d^{-1}. The seepage rate mirrored the water depth very well and was negatively correlated with salinity around the spring tide, while there was no apparent trend with salinity around the neap tide (Figure S12, SI). The maximum rate, 25 cm d^{-1}, occurred at the lowest water depth during the spring tide on February 7. Our study indicated that even in the dry season the effect of tidal pumping on SGD was striking during the spring tide in coastal fringing reefs.

4.4. Impacts of SGD on the Coastal Coral Reef System. During the spring tide pH was predominantly affected by SGD input during ebb flows and mainly controlled by biological activities during flood tides (Figure 4d), while during the neap tide pH was affected mostly by biological activities with a 100% contribution on February 12. The pH was as low as 7.72 during the spring tide, which was due to SGD inputs into the coral reef system. This implied that SGD might pose a potential threat to this coral reef system. Such low pH is severely detrimental to calcifier recruitment and reef builders.[4] Our study revealed quantitatively how SGD and biological activities affected pH on diel and tidal scales. In coral lagoons at Rarotonga, SGD was the dominant driver of pH at low tides, while at Heron Island biological activities were predominant in the afternoons.[15] SGD-derived high fluxes of free CO_2 are a positive feedback to ocean acidification in coral reef systems,[15] even though SGD often has high TA concentrations. In our reef system SGD actually lowered the buffering capacity as reflected by the Revelle Factor (Figure S13, SI).

The aragonite saturation state (Ω), the ratio of the ion product to the solubility product constant, in this coral reef system varied with tides (Figure 4e), with the lowest value of 1.77 during the spring tide, corresponding to the minimum pH of 7.72. The community calcification rate has been demonstrated to drop to 0 when $\Omega_{aragonite}$ = 1.7 ± 0.2.[4] Although at Station CT this low $\Omega_{aragonite}$ did not last long in a spring-neap tidal cycle, periodic acidification during the spring tide due to SGD input might impede calcification of the community in the long run.

4.5. Future Scenarios under Higher Atmospheric CO_2. In the global context of increasing atmospheric CO_2, it is expected that surface seawater pH will further decrease by 0.3–0.4 pH units, if atmospheric CO_2 concentrations reach 800 ppmv by the end of the century.[29] Coastal fringing reef systems, under the influence of tidal-driven SGD, would be more vulnerable to this atmospheric CO_2 rise. Assuming that the fraction of SGD water, the SGD inputs of DIC and TA, and the biologically contributed DIC and TA stayed unchanged, the saturation state of aragonite and pH would drop significantly when being equilibrated with increasing atmospheric CO_2 (Figure 5). At the minimum depth during the spring tide when the atmospheric CO_2 concentration increases to 436 ppmv (a value reached in 20 yrs considering a very conservative

dx.doi.org/10.1021/es5026867 | Environ. Sci. Technol. 2014, 48, 13069–13075

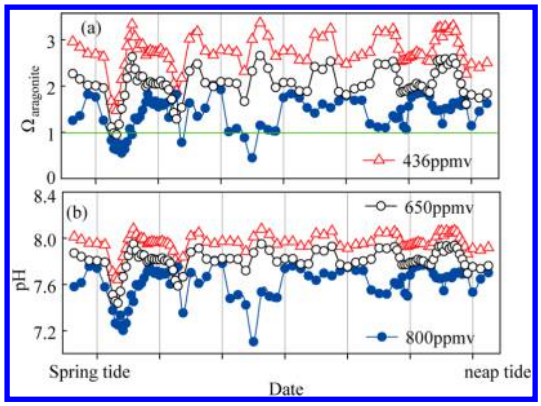

Figure 5. Predicted diurnal changes in the saturation state of aragonite ($\Omega_{aragonite}$) and pH in a spring-neap tidal cycle in scenarios of increasing atmospheric CO_2 at concentrations of 436 ppmv, 650 ppmv and 800 ppmv. (a) $\Omega_{aragonite}$, (b) pH.

rate of increase, 1.9 ppm yr^{-1}, the average rate in 1995–2005[30]), the saturation state of aragonite would decrease from 1.77 to 1.47 and pH would decrease from 7.72 to 7.64. When the atmospheric CO_2 reaches 650 ppmv, the predicted value in 2060 under the worst case emission scenario,[31] the saturation state of aragonite would reach 0.95 at the minimum water depth during the spring tide and the undersaturation (Ω <1) would last for at least an hour with the lowest pH of 7.44. The scenario would become even worse at the end of the century, if atmospheric CO_2 reached 800 ppmv. In a spring to neap tidal cycle, with pH ≤7.81 Ω would be less than 2 for most of the tidal cycle. Around the spring tide, pH would be as low as 7.18 and aragonite would be undersaturated for 8 h. Corals exposed to undersaturated waters around springs were already observed to decrease in skeletal density and increase in susceptibility to bioerosion.[32]

Besides increasing atmospheric CO_2, sea-level rise and potential changes of water head in coastal aquifers due to climate change may affect the magnitude of SGD[33] through changing the hydraulic gradient. In addition, thermal stress on fringing reefs due to global warming may cause reef bleaching.[17] Along with the anticipated increase of nutrient loads to watersheds, organic loading would also be expected to continually grow in the shallow groundwater, which would inevitably make the groundwater more acidic. Therefore, coral reef systems under the influence of SGD will most likely be more susceptible to climate change than those with no or minimal SGD inputs.

■ ASSOCIATED CONTENT

Ⓢ Supporting Information

Sampling and measurements, groundwater data, how to estimate SGD rates using ^{226}Ra and Darcy's law, and how to quantitatively differentiate contributions of SGD and biological activities and of inorganic and organic carbon metabolism to the carbonate system parameters, including three tables (Tables S1–S3) and 13 figures (Figures S1–S13). This material is available free of charge via the Internet at http://pubs.acs.org.

■ AUTHOR INFORMATION

Corresponding Author

*Phone: 0086-592-2182132; fax: 0086-592-2184101; e-mail: mdai@xmu.edu.cn.

Author Contributions

The manuscript was written through the contribution of all authors. All authors have given approval to the final version of the manuscript.

Notes

The authors declare no competing financial interest.

■ ACKNOWLEDGMENTS

We thank the crew on the ship *Qionglingao 02706* and Junde Dong for arranging local logistic support at the Tropical Marine Biological Research Station, Chinese Academy of Sciences in Hainan. We are grateful to Willard Moore, Wei-Jun Cai, and Zong-Pei Jiang for helpful discussion and to three anonymous reviewers for their critical and constructive comments that have helped improve the manuscript. John Hodgkiss is thanked for polishing the English. This study was funded by the National Basic Research Program of China (2009CB421200), the Ministry of Science and Technology of China (2011IM010700), the National Natural Science Foundation of China (NSFC) (41006041), and the Science Fund for Creative Research Groups of NSFC (41121091). This paper is in memory of Wenping Jing, an outstanding master student who sorrowfully passed away on January 16, 2013.

■ REFERENCES

(1) Le Quéré, C.; Peters, G. P.; Andres, R. J.; Andrew, R. M.; Boden, T. A.; Ciais, P.; Friedlingstein, P.; Houghton, R. A.; Marland, G.; Moriarty, R.; Sitch, S.; Tans, P.; Arneth, A.; Arvanitis, A.; Bakker, D. C. E.; Bopp, L.; Canadell, J. G.; Chini, L. P.; Doney, S. C.; Harper, A.; Harris, I.; House, J. I.; Jain, A. K.; Jones, S. D.; Kato, E.; Keeling, R. F.; Klein Goldewijk, K.; Körtzinger, A.; Koven, C.; Lefèvre, N.; Maignan, F.; Omar, A.; Ono, T.; Park, G.-H.; Pfeil, B.; Poulter, B.; Raupack, M. R.; Regnier, P.; Rödenbeck, C.; Saito, S.; Schwinger, J.; Segschneider, J.; Stocker, B. D.; Takahashi, T.; Tilbrook, B.; van Heuven, S.; Viovy, N.; Wanninkhof, R.; Wiltshire, A.; Zaehle, S. Global carbon budget 2013. *Earth Syst. Sci. Data* **2014**, *6*, 235–263.

(2) Chen, G.-T.; Millero, F. Gradual increase of oceanic CO_2. *Nature* **1979**, *277*, 205–206.

(3) Doney, S. C.; Fabry, V. J.; Feely, R. A.; Kleypas, J. A. Ocean acidification: The other CO_2 problem. *Annu. Rev. Mar. Sci.* **2009**, *1*, 169–92.

(4) Kleypas, J. A.; Langdon, C. Coral reefs and changing seawater carbonate chemistry. *Coastal Estuarine Stud.* **2006**, *61*, 73–110.

(5) Feely, R. A.; Sabine, C. L.; Hernandez-Ayon, J. M.; Ianson, D.; Hales, B. Evidence for upwelling of corrosive″ acidified″ water onto the continental shelf. *Science* **2008**, *320*, 1490–1492.

(6) Hall-Spencer, J. M.; Rodolfo-Metalpa, R.; Martin, S.; Ransome, E.; Fine, M.; Turner, S. M.; Rowley, S. J.; Tedesco, D.; Buia, M.-C. Volcanic carbon dioxide vents show ecosystem effects of ocean acidification. *Nature* **2008**, *454*, 96–99.

(7) Carpenter, K. E.; Abrar, M.; Aeby, G.; Aronson, R. B.; Banks, S.; Bruckner, A.; Chiriboga, A.; Cortés, J.; Delbeek, J. C.; DeVantier, L. One-third of reef-building corals face elevated extinction risk from climate change and local impacts. *Science* **2008**, *321*, 560–563.

(8) Liu, S.; Li, R.; Zhang, G.; Wang, D.; Du, J.; Herbeck, L. C.; Zhang, J.; Ren, J. The impact of anthropogenic activities on nutrient dynamics in the tropical Wenchanghe and Wenjiaohe Estuary and Lagoon system in East Hainan, China. *Mar. Chem.* **2011**, *125*, 49–68.

(9) Santos, I. R.; Glud, R. N.; Maher, D.; Erler, D.; Eyre, B. D. Diel coral reef acidification driven by porewater advection in permeable carbonate sands, Heron Island, Great Barrier Reef. *Geophys. Res. Lett.* **2011**, *38*, L03604, DOI: 10.1029/2010GL046053.

(10) Moore, W. S. The effect of submarine groundwater discharge on the ocean. *Annu. Rev. Mar. Sci.* **2010**, *2*, 59–88.

(11) Cai, W.-J.; Wang, Y.; Krest, J.; Moore, W. The geochemistry of dissolved inorganic carbon in a surficial groundwater aquifer in North

Inlet, South Carolina, and the carbon fluxes to the coastal ocean. *Geochim. Cosmochim. Acta* **2003**, *67*, 631−639.
(12) Liu, Q.; Charette, M. A.; Henderson, P. B.; McCorkle, D. C.; Martin, W.; Dai, M. Effect of submarine groundwater discharge on the coastal ocean inorganic carbon cycle. *Limnol. Oceanogr.* **2014**, *59*, 1529−1554.
(13) Cyronak, T.; Santos, I. R.; Erler, D. V.; Eyre, B. D. Groundwater and porewater as major sources of alkalinity to a fringing coral reef lagoon (Muri Lagoon, Cook Islands). *Biogeosciences* **2013**, *10*, 2467−2480.
(14) Santos, I. R.; Erler, D.; Tait, D.; Eyre, B. D. Breathing of a coral cay: Tracing tidally driven seawater recirculation in permeable coral reef sediments. *J. Geophys. Res.* **2010**, *115*, C12010, DOI: 10.1029/2010JC006510.
(15) Cyronak, T.; Santos, I. R.; Erler, D. V.; Maher, D. T.; Eyre, B. D., Drivers of pCO_2 variability in two contrasting coral reef lagoons: The influence of submarine groundwater discharge. *Global Biogeochem. Cycles* **2014**, *28*, DOI: 10.1002/2013GB004598.
(16) Zhang, Q. On biogeomorphology of Luhuitou fringing reef of Sanya city, Hainan Island, China. *Chin. Sci. Bull.* **2001**, *46*, 97−101.
(17) Zhao, M.; Yu, K.; Zhang, Q.; Shi, Q.; Price, G. J. Long-term decline of a fringing coral reef in the northern South China Sea. *J. Coast. Res.* **2012**, *28*, 1088−1099.
(18) Li, X.; Liu, S.; Huang, H.; Huang, L.; Jing, Z.; Zhang, C. Coral bleaching caused by an abnormal water temperature rise at Luhuitou fringing reef, Sanya Bay, China. *Aquat. Ecosyst. Health Manage.* **2012**, *15*, 227−233.
(19) Zhang, C.; Huang, H.; Ye, C.; Huang, L.; Li, X.; Lian, J.; Liu, S. Diurnal and seasonal variations of carbonate system parameters on Luhuitou fringing reef, Sanya Bay, Hainan Island, South China Sea. *Deep-Sea Res., Part II* **2013**, *96*, 65−74.
(20) Wang, H.; Dong, J.; Wang, Y.; Chen, G.; Zhang, Y. Variations of nutrient contents and their transportation estimate at Sanya Bay. *J. Trop. Oceanogr.* **2005**, *25*, 90−95 (in Chinese).
(21) Li, X.-b.; Huang, H.; Lian, J.-s.; Liu, S.; Huang, L.-M.; Yang, J.-h. Spatial and temporal variations in sediment accumulation and their impacts on coral communities in the Sanya Coral Reef Reserve, Hainan, China. *Deep-Sea Res., Part II* **2013**, *96*, 88−96.
(22) Wu, M.-L.; Zhang, Y.-Y.; Dong, J.-D.; Cai, C.-H.; Wang, Y.-S.; Long, L.-J.; Zhang, S. Monsoon-driven dynamics of environmental factors and phytoplankton in tropical Sanya Bay, South China sea. *Oceanol. Hydrobiol. Stud.* **2012**, *41*, 57−66, DOI: 10.2478/s13545-012-0007-1.
(23) Zhou, W.; Li, T.; Cai, C.; Huang, L.; Wang, H.; Xu, J.; Dong, J.; Zhang, S. Spatial and temporal dynamics of phytoplankton and bacterioplankton biomass in Sanya Bay, northern South China Sea. *J. Environ. Sci.* **2009**, *21*, 595−603.
(24) Huang, L.; Tan, Y.; Song, X.; Huang, X.; Wang, H.; Zhang, S.; Dong, J.; Chen, R. The status of the ecological environment and a proposed protection strategy in Sanya Bay, Hainan Island, China. *Mar. Pollut. Bull.* **2003**, *47*, 180−186.
(25) Zhao, X.; Peng, G.; Zhang, J. A preliminary study of Holocene stratigraphy and sea level changes along the coast of Hainan Island. *Chin. J. Geology* **1979**, *4*, 350−358 (in Chinese).
(26) Zhang, Z.; Liu, R.; Han, Z. The quaternary stratigraphy along the coastal area of Hainan Island. *Trop. Geogr.* **1987**, *7*, 54−64 (in Chinese).
(27) Dai, M.; Lu, Z.; Zhai, W.; Chen, B.; Cao, Z.; Zhou, K.; Cai, W.-J.; Chen, C.-T. A. Diurnal variations of surface seawater pCO_2 in contrasting coastal environments. *Limnol. Oceanogr.* **2009**, *54*, 735−745.
(28) Jiang, Z.-P.; Huang, J.-C.; Dai, M.; Kao, S. J.; Hydes, D. J.; Chou, W.-C.; Jan, S. Short-term dynamics of oxygen and carbon in productive nearshore shallow seawater systems off Taiwan: Observations and modeling. *Limnol. Oceanogr.* **2011**, *56*, 1832−1849.
(29) Orr, J. C.; Fabry, V. J.; Aumont, O.; Bopp, L.; Doney, S. C.; Feely, R. A.; Gnanadesikan, A.; Gruber, N.; Ishida, A.; Joos, F. Anthropogenic ocean acidification over the twenty-first century and its impact on calcifying organisms. *Nature* **2005**, *437*, 681−686.
(30) IPCC. *Climate change 2007. Synthesis Report. Contribution of Working Groups I, II and III to the Fourth Assessment Report*; IPCC: Geneva, Switzerland, 2008.
(31) Houghton, J. T.; Ding, Y.; Griggs, D. J.; Noguer, M.; van der LINDEN, P. J.; Dai, X.; Maskell, K.; Johnson, C. *Climate Change 2001: The Scientific Basis. Contribution of Working Group I to the Third Assessment Report of the Intergovenmental Panel on Climate Change*; Cambridge University Press: Cambridge, UK, 2001.
(32) Crook, E. D.; Cohen, A. L.; Rebolledo-Vieyra, M.; Hernandez, L.; Paytan, A. Reduced calcification and lack of acclimatization by coral colonies growing in areas of persistent natural acidification. *Proc. Natl. Acad. Sci. U.S.A.* **2013**, *110*, 11044−11049.
(33) Gonneea, M. E.; Mulligan, A. E.; Charette, M. A. Climate-driven sea level anomalies modulate coastal groundwater dynamics and discharge. *Geophys. Res. Lett.* **2013**, *40*, 2701−2706.